Asociación Argentina de Mecánica Computacional

Mecánica Computacional Vol XXXI, págs. 1799-1819 (artículo completo)
Alberto Cardona, Paul H. Kohan, Ricardo D. Quinteros, Mario A. Storti (Eds.)
Salta, Argentina, 13-16 Noviembre 2012

A COMPARISON OF EFFECTIVE PROPERTIES OF NODULAR CAST-IRON CONSIDERING DIFFERENT SHAPES OF THE REPRESENTATIVE VOLUME ELEMENT

Adrián D. Boccardo[a], **Fernando D. Carazo**[b] **and Sebastián M. Giusti**[c]

[a]*CIII - Departamento de Ingeniería Mecánica, Universidad Tecnológica Nacional - Facultad Regional Córdoba, Maestro M. Lopéz esq. Cruz Roja Argentina, Ciudad Universitaria, Córdoba, Argentina, aboccardo@mecanica.frc.utn.edu.ar, http://www.frc.utn.edu.ar*

[b]*Instituto de Investigaciones Antisísmicas Ing. Aldo Bruschi, Facultad de Ingeniería, Universidad Nacional de San Juan, Av. Libertador Gral. San Martín 1290(O), San Juan, Argentina, fcarazo@unsj.edu.ar, http://www.idia.unsj.edu.ar*

[c]*Departamento de Ingeniería Civil, Universidad Tecnológica Nacional - Facultad Regional Córdoba, Maestro M. Lopéz esq. Cruz Roja Argentina, Ciudad Universitaria, Córdoba, Argentina - CONICET, sgiusti@civil.frc.utn.edu.ar, http://www.frc.utn.edu.ar*

Keywords: Multi-scale modeling, Material characterization, Nodular cast iron, Finite element, Representative volume element hexagonal and rectangular.

Abstract. In the present work we use a numerical approach based on a computational constitutive multiscale model to predict the effective Young's modulus and the Poisson ratio of a perlitic nodular cast iron. In order to obtain the Representative Volume Element (RVE), we use a set of micrographies acquired from an optical device. For each micrograph we define two RVE with different shape, rectangular and hexagonal. The volumetric fraction of graphite and metal matrix and the boundary of each object were identified on each RVE by using a procedure of image enhanced and segmentation. These set of RVE was meshed with triangular finite elements. The numerical results obtained from both RVE are compared and discussed with results obtained with an analytical expression. Finally, some conclusions are presented.

1 INTRODUCTION

Cast irons are a Fe-C-Si alloy with $3.0 - 4.3\%C$ and $1.3 - 3.0\%Si$. The high carbon content determines the mechanical properties based in the retained carbon in the solid solution at room temperature, while silicon promotes the precipitation of carbon in the form of graphite.

At present, cast irons are manufactured in larger quantities than any other type of cast alloy (Panchal, 2010), and in some cases they have replaced steel castings. This is mainly due to their lower melting point, and high carbon content which improves the castability and fluidity during the pouring process. Others important properties of cast iron are the lower levels of defects produced during the filling of a mold and a wide range of mechanical properties as indicated in the Table 1. There are two main factors that control these properties: *(a)* type, size and size distribution of graphite nodules, and; *(b)* type of matrix and defects present: ferrite/pearlite relation, its own characteristic and the presence of microstructural defects.

Grade	Tensile Strength (MPa)	Yield Strength (MPa)	Hardness(HB)	Elongation (%)
$60-40-18$	42000	28000	$149-187$	18
$65-45-12$	45000	32000	$170-207$	12
$80-55-06$	56000	38000	$187-255$	6
$100-70-03$	70000	47000	$217-267$	3
$120-70-02$	84000	63000	$240-300$	2

Table 1: Mechanical properties of SGI's (spheroidal graphite iron) according to ASTM A536.

The goal of the metallurgist is to design a process producing a microstructure which yields the expected mechanical properties. This requires knowledge of the relations between microstructure and mechanical properties in alloys as well as identification of the factors affecting the microstructure. Actually, the use of RVE in the context of micro-mechanics is commonly used to determine the effective properties of materials. Thus, a proper choice of the RVE is decisive in the study of materials, from the point of view of the principles and laws of the micro-mechanics and multi-scale theories. In general, an RVE should be characterized by: *(a)* to be statistically representative of the macro-scopic response of the continuum, and *(b)* its dimension must be larger than the minimum size of the heterogeneity that characterizes the microstructure of the material. However there are numerous definitions of RVE (Hill, 1963; Hashin, 1983; Drugan and Willis, 1996; Trusov and Keller, 1997; van Mier, 1997; Evesque, 2000; Gitman et al., 2007), in general, an RVE can be considered as the minimum volume of material whose behavior is equivalent to a volume of a homogeneous fictitious material.

From an engineering point of view, the main applications and uses of RVE are: *(a)* the modeling and study of the influence of heterogeneities at the nano, micro and meso-structural level (localization) and *(b)* the obtaining of the effective properties from the properties of micro-constituents (homogenization).

From the above mentioned, we highlights the importance of an adequate representation of a material by an RVE. There are two prevailing philosophies for generating the RVE for heterogeneous finite element modeling: *(a)* synthetic microstructures, usually obtained from computer algorithms, and *(b)* microstructure obtained directly from experiments conducted in the laboratory. Most papers in research fields related with multi-scale theories and effective properties of alloys are based on RVE obtained from synthetic techniques. Therefore, the microstructures are characterized by periodic idealized microgeometries, such as classic arrays composed of cubic spheres embedded in a homogeneous matrix and idealized form of cylinders with varying aspect ratios (Rintoul and Torquato, 1997; Torquato, 1998; Bochenek and Pyrz, 2002; Zeman and Sejnoha, 2001; Roberts and Garboczi, 1999). The RVE obtained by this way are applicable only in cases where the microstructure consists of periodic arrays characterized by homogeneous, uniform and one size heterogeneities. In general, in the alloys (including a large number of composite materials) the microstructure does not satisfy these requirements. A clear example is the alloy studied in this paper, SGI. Figure 1 show two micrographs corresponding at two different points of a melt part which have different cooling rates. Can be observed a non-uniform distribution of the “spheres” of graphite (which correspond to the black color phase in both figures), much less a constant size and shape. These quantities are of great importance in the effective properties of a continuous medium (Bohm et al., 1994; Deve, 1999).

On the other hand, there are numerous papers in which the RVE are obtained from micrographs (Terada and Kikuchi, 1996; Fischmeister and Karlsson, 1977; Li et al., 1999; Ghosh and Moorthy, 1995; Berryman and Blair, 1987; Hollister and Kikuchi, 1994), but none of these cases corresponds to metallic alloys.

In the case of SGI, the importance to obtain an adequate RVE from the micrographs is evidenced by observing and comparing the micrographs shown in Figures 1(a) and 1(b). There are several differences in the size distribution of graphite nodules, the presence of micropores, and graphite nodules of low quality. All these properties affect the quality of the alloys by contributing to generate crack initiation zones and concentrations of stresses and strains at the micro-level. In this paper the concept of RVE is used in the sense of "statistical volume element" (Ostoja-Starzewski, 2006). Another interpretation from which the RVE proposed in this paper can be considered periodic, is given by (Drugan and Willis, 1996), where the RVE can be considered as the volume element for which the macro-scopic constitutive properties are precise enough to represent the overall constitutive response of the continuum medium. Then, a RVE can be considered valid if the moduli values are within of the 5% of the value of the module given at macro-scopic level. At this point, takes a great preponderance determines upper and lower bounds in the effective properties calculated from the RVE.

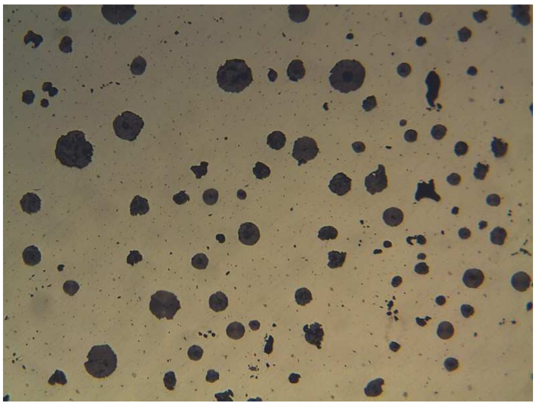

(a)

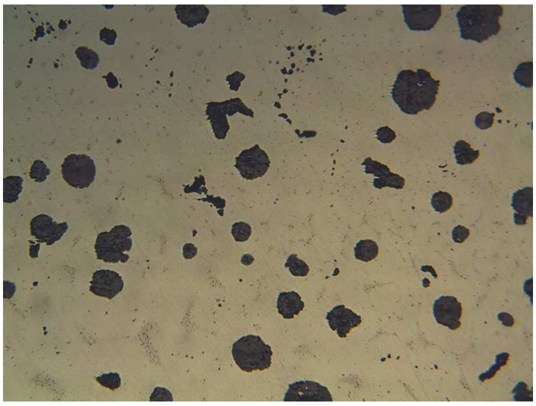

(b)

Figure 1: Micrographies of semipearlitic SGI corresponding ar two differents points.

This work presents a comprehensive methodology to determines the effective properties in heterogeneous continuum medium from micrographs, which involves the combination of digital image processing and quantification and characterization of microstructure. The main scope of this paper is to compare the numerical results obtained from numerical simulations carried out with two RVE shape: rectangular and hexagonal. To achieve this objective we presents a computational constitutive multi-scale model to predict elastic constants such as Young's modulus of a pearlitic SGI by taking into account the influence of graphite, matrix volumetric phase fractions, and nodularity of samples used in the study. Numerical values are compared with results obtained from an analytical formula (Mazilu and Ondracek, 1990).

2 MULTI-SCALE MODELING

This section presents a summary of the multi-scale constitutive theory upon which we rely for the estimation of the macro-scopic elasticity properties. This family of (now well established) constitutive theories has been formally presented in a rather general setting by Germain et al. (1983) and later explorated, among others, by Michel et al. (1999) and Miehe et al. (1999) in the computational context. When applied to the modeling of linearly elastic periodic media, it coincides with the asymptotic expansion-based theory described by Bensoussan et al. (1978) and Sanchez-Palencia (1980).

The starting point of this family of constitutive theories is the assumption that any point $\boldsymbol{x}$ of the macro-scopic continuum is associated to a local RVE whose domain Ω_μ, with boundary $\partial\Omega_\mu$, has characteristic length l_μ, much smaller than the characteristic length l of the macro-continuum domain Ω, as hown in Figure 2. For simplicity, we consider that the RVE domain consists of a matrix, Ω_μ^m, containing inclusions of different materials occupying a domain Ω_μ^i (see Figure 2).

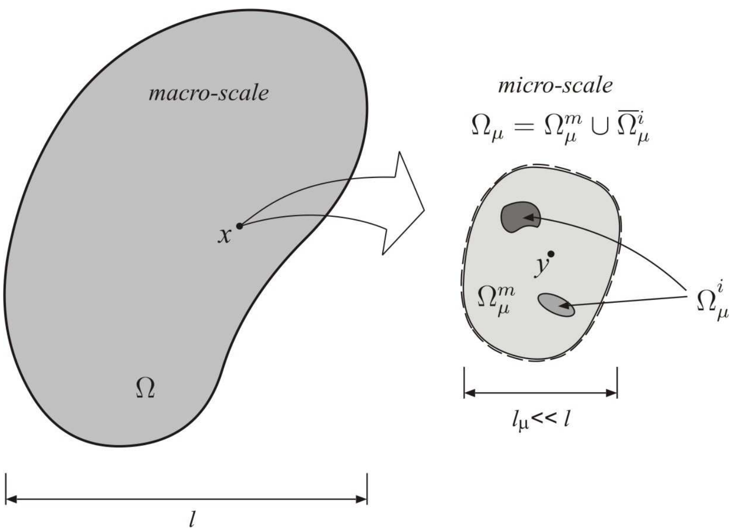

Figure 2: Macro-scopic continuum with a locally RVE.

An axiomatic variational framework for this family of constitutive theories is presented in detail by de Souza Neto and Feijóo (2006). Accordingly, the entire theory can be derived from five basic principles: (1) The strain averaging relation; (2) A simple further constraint upon the possible functional sets of cinematically admissible displacement fields of the RVE; (3) The equilibrium of the RVE; (4) The stress averaging relation; (5) The Hill-Mandel Principle of Macro-Homogeneity, which ensures the energy consistency between the so-called micro and macro-scales of the material. These are briefly stated in the following.

The first basic axiom – the strain averaging relation – states that the macro-scopic strain tensor $\mathbf{E}$ at a point $\boldsymbol{x}$ of the macro-scopic continuum is the volume average of its micro-scopic counterpart $\mathbf{E}_\mu$ over the domain of the RVE:

$$\mathbf{E} := \frac{1}{V_\mu}\int_{\Omega_\mu} \mathbf{E}_\mu \tag{1}$$

where V_μ is a total volume of the RVE and

$$\mathbf{E}_\mu := \nabla^s \mathbf{u}_\mu \tag{2}$$

with $\mathbf{u}_\mu$ denoting the micro-scopic displacement field of the RVE. Equivalently, in terms of RVE boundary displacements, the homogenized strain (Equation 1 and 2) can be written as

$$\mathbf{E} = \frac{1}{V_\mu}\int_{\partial\Omega_\mu} \mathbf{u}_\mu \otimes_s \mathbf{n} \tag{3}$$

where $\mathbf{n}$ is the outward unit normal to the boundary $\partial\Omega_\mu$ and $\otimes_s$ denotes the symmetric tensor product.

As a result of axiom (Equation 1) and, in addition, by requiring without loss of generality that the volume average of the micro-scopic displacement field coincides with the macro-scopic displacement $\mathbf{u}$, any chosen set $\mathcal{K}_\mu$ of admissible displacement fields of the RVE must satisfy

$$\mathcal{K}_\mu \subset \mathcal{K}^*_\mu := \left\{ \boldsymbol{v} \in \left[H^1(\Omega_\mu)\right]^2 : \int_{\Omega_\mu} \boldsymbol{v} = V_\mu \mathbf{u}\,, \int_{\partial\Omega_\mu} \boldsymbol{v} \otimes_s \mathbf{n} = V_\mu\, \mathbf{E},\ [\![\boldsymbol{v}]\!] = \mathbf{0} \text{ on } \partial\Omega^i_\mu \right\} \tag{4}$$

where $\mathcal{K}^*_\mu$ is the *minimally constrained set of cinematically admissible RVE displacement fields* and $[\![\boldsymbol{v}]\!]$ denotes the *jump* of function $\boldsymbol{v}$ across the matrix/inclusion interface $\partial\Omega^i_\mu$, defined as

$$[\![(\cdot)]\!] := (\cdot)|_m - (\cdot)|_i \tag{5}$$

with subscripts m and i associated, respectively, with quantity values on the matrix and inclusion. Now, without loss of generality, $\mathbf{u}_\mu$ may be decomposed as a sum

$$\mathbf{u}_\mu\left(\boldsymbol{y}\right) = \mathbf{u} + \bar{\mathbf{u}}\left(\boldsymbol{y}\right) + \tilde{\mathbf{u}}_\mu\left(\boldsymbol{y}\right) \tag{6}$$

of a constant (rigid) RVE displacement coinciding with the macro-displacement $\mathbf{u}$, a field $\bar{\mathbf{u}}\left(\boldsymbol{y}\right) := \mathbf{E}\,\boldsymbol{y}$, linear in the local RVE coordinate $\boldsymbol{y}$ (whose origin is assumed without loss of generality to be located at the centroid of the RVE) and a fluctuation displacement field $\tilde{\mathbf{u}}_\mu(\boldsymbol{y})$ that, in general, varies with $\boldsymbol{y}$. With the above split, the micro-scopic strain field (Equation 2) can be written as a sum of a homogeneous strain (uniform over the RVE) coinciding with the macro-scopic strain and a field $\tilde{\mathbf{E}}_\mu := \nabla^s \tilde{\mathbf{u}}$ corresponding to a fluctuation of the micro-scopic strain about the homogenized (average) value.

$$\mathbf{E}_\mu = \mathbf{E} + \tilde{\mathbf{E}}_\mu \tag{7}$$

The additive split (Equation 6) allows the constraint (Equation 4) to be expressed in terms of displacement fluctuations alone. It is equivalent to requiring that the (as yet to be defined) set $\tilde{\mathcal{K}}_\mu$ of admissible displacement fluctuations of the RVE be a subset of the *minimally constrained space of displacement fluctuations*, $\tilde{\mathcal{K}}^*_\mu$:

$$\tilde{\mathcal{K}}_\mu \subset \tilde{\mathcal{K}}^*_\mu := \left\{ \boldsymbol{v} \in \left[H^1(\Omega_\mu)\right]^2 : \int_{\Omega_\mu} \boldsymbol{v} = \mathbf{0}, \int_{\partial\Omega_\mu} \boldsymbol{v} \otimes_s \mathbf{n} = \mathbf{0},\ [\![\boldsymbol{v}]\!] = \mathbf{0} \text{ on } \partial\Omega^i_\mu \right\} \tag{8}$$

At this point we introduce the further assumption that $\tilde{\mathcal{K}}_\mu$ is a *subspace* of $\tilde{\mathcal{K}}^*_\mu$. Then, we have that the space of *virtual displacement* of the RVE, defined as

$$\mathcal{V}_\mu := \left\{\boldsymbol{\eta} \in \left[H^1(\Omega_\mu)\right]^2 : \boldsymbol{\eta} = \boldsymbol{v}_1 - \boldsymbol{v}_2;\ \forall \boldsymbol{v}_1, \boldsymbol{v}_2 \in \mathcal{K}_\mu\right\} \tag{9}$$

coincides with the space of micro-scopic displacement fluctuations, i.e.,

$$\mathcal{V}_\mu = \tilde{\mathcal{K}}_\mu \tag{10}$$

The next axiom establishes that the macro-scopic stress tensor $\mathbf{T}$ is given by the volume average of the micro-scopic stress field $\mathbf{T}_\mu$ over the RVE, i.e.,

$$\mathbf{T} := \frac{1}{V_\mu}\int_{\Omega_\mu} \mathbf{T}_\mu \tag{11}$$

The present paper is focused on RVEs whose matrix and inclusion materials are described by the classical isotropic linear elastic constitutive law. That is, the micro-scopic stress tensor field $\mathbf{T}_\mu$ satisfies

$$\mathbf{T}_\mu = \mathbb{C}_\mu \mathbf{E}_\mu \tag{12}$$

where $\mathbb{C}_\mu$ is the fourth order isotropic elasticity tensor:

$$\mathbb{C}_\mu = \frac{E}{1-\nu^2}\left[(1-\nu)\,\mathbb{I} + \nu\,(\mathbf{I}\otimes\mathbf{I})\right] \tag{13}$$

with E and ν denoting, respectively, the Young's modulus and the Poisson's ratio. These parameters are given by

$$E := \begin{cases} E_m & \text{if} \quad \boldsymbol{y} \in \Omega_\mu^m \\ E_i & \text{if} \quad \boldsymbol{y} \in \Omega_\mu^i \end{cases} \quad \text{and} \quad \nu := \begin{cases} \nu_m & \text{if} \quad \boldsymbol{y} \in \Omega_\mu^m \\ \nu_i & \text{if} \quad \boldsymbol{y} \in \Omega_\mu^i \end{cases} \tag{14}$$

The parameters E_i and ν_i constant within each inclusion but may in general vary from inclusion to inclusion. In Equation 13 we use $\mathbf{I}$ and $\mathbb{I}$ to denote the second and fourth order identity tensors, respectively.

The linearity of Equation 12 together with the additive decomposition indicated in Equation 7 allows the micro-scopic stress field to be split as

$$\mathbf{T}_\mu = \bar{\mathbf{T}}_\mu + \tilde{\mathbf{T}}_\mu \tag{15}$$

where $\bar{\mathbf{T}}_\mu$ is the stress field associated with the uniform strain induced by $\bar{\mathbf{u}}\,(\boldsymbol{y})$, i.e., $\bar{\mathbf{T}}_\mu = \mathbb{C}_\mu \mathbf{E}$, and $\tilde{\mathbf{T}}_\mu$ is the stress fluctuation field associated with $\tilde{\mathbf{u}}_\mu\,(\boldsymbol{y})$, i.e., $\tilde{\mathbf{T}}_\mu = \mathbb{C}_\mu \tilde{\mathbf{E}}$.

A further axiom of the theory is the so-called Hill-Mandel Principle of Macro-Homogeneity (Hill (1965) and Mandel (1971)). This principle establishes that the power of the macro-scopic stress tensor at an arbitrary point of the macro-continuum must equal the volume average of the power of the micro-scopic stress over the RVE associated with that point for any cinematically admissible motion of the RVE.

The general theory is completed by a final axiom which establishes that the RVE must satisfy equilibrium. Then, with the introduction of Equation 15 into the classical virtual work variational equation, we have that the *RVE mechanical equilibrium problem* consists of finding, for a given macro-scopic strain $\mathbf{E}$, a cinematically admissible micro-scopic displacement fluctuation field $\tilde{\mathbf{u}}_\mu \in \mathcal{V}_\mu$, such that

$$\int_{\Omega_\mu} \tilde{\mathbf{T}}_\mu \cdot \nabla^s \boldsymbol{\eta} = -\int_{\Omega_\mu} \bar{\mathbf{T}}_\mu \cdot \nabla^s \boldsymbol{\eta} \quad \forall \boldsymbol{\eta} \in \mathcal{V}_\mu \tag{16}$$

2.1 Classes of multi-scale constitutive models

The characterization of a multi-scale model of the present type is completed with the choice of a suitable space of cinematically admissible displacement fluctuations $\mathcal{V}_\mu \subset \tilde{\mathcal{K}}_\mu^*$. We list below the four classical possible choices:

- *Homogeneous strain model or Taylor model*. For this class of models the choice is

$$\mathcal{V}_\mu = \mathcal{V}_\mu^{\mathcal{T}} := \left\{ \tilde{\mathbf{u}}_\mu \in \tilde{\mathcal{K}}_\mu^* : \tilde{\mathbf{u}}_\mu(\boldsymbol{y}) = \mathbf{0} \; \forall \boldsymbol{y} \in \partial\Omega_\mu \right\} \tag{17}$$

  In this case, the strain is homogeneous over the RVE, i.e. $\mathbf{E}_\mu = \mathbf{E}$ in Ω_μ. The reactive RVE body force and external traction fields, $(\mathbf{q}_\mu, \mathbf{b}_\mu) \in \left(\mathcal{V}_\mu^{\mathcal{T}}\right)^\perp$, may be arbitrary functions.

- *Linear boundary displacement model*. For this class of models the choice is

$$\mathcal{V}_\mu = \mathcal{V}_\mu^{\mathcal{L}} := \left\{ \tilde{\mathbf{u}}_\mu \in \tilde{\mathcal{K}}_\mu^* : \tilde{\mathbf{u}}_\mu(\boldsymbol{y}) = \mathbf{0} \; \forall \boldsymbol{y} \in \partial\Omega_\mu \right\} \tag{18}$$

  The only possible reactive body force over Ω_μ orthogonal to $\mathcal{V}_\mu^{\mathcal{L}}$ is $\mathbf{b}_\mu = \mathbf{0}$. On $\partial\Omega_\mu$, the resulting reactive external traction, $\mathbf{q}_\mu \in \left(\mathcal{V}_\mu^{\mathcal{L}}\right)^\perp$, may be any function.

- *Periodic boundary fluctuations model*. This class of models is typical of the analysis of periodic media, where the macro-scopic continuum is generated by the repetition of the RVE. In this case, the geometry of the RVE must satisfy certain geometrical constraints not needed by the other two classes discussed here. Considering for simplicity the case of polygonal RVE geometries (see Figure 3), we have that the boundary $\partial\Omega_\mu$ is composed of a number of pairs of equally-sized subsets $\{\Gamma_i^+, \Gamma_i^-\}$ with normals $\mathbf{n}_i^+ = -\mathbf{n}_i^-$. For each pair $\{\Gamma_i^+, \Gamma_i^-\}$ of sides there is a one-to-one correspondence between points $\boldsymbol{y}^+ \in \Gamma_i^+$ and $\boldsymbol{y}^- \in \Gamma_i^-$.

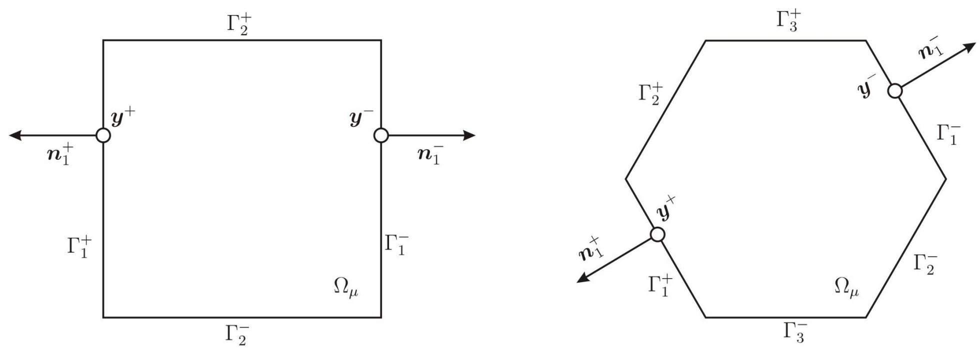

Figure 3: Typical RVE geometries for periodic media.

  The periodicity of the structure requires that the displacement fluctuation at any point $\boldsymbol{y}^+$ coincide with that of the corresponding point $\boldsymbol{y}^-$. Hence, the space of displacement fluctuations is defined as

$$\mathcal{V}_\mu = \mathcal{V}_\mu^{\mathcal{P}} := \left\{ \tilde{\mathbf{u}}_\mu \in \tilde{\mathcal{K}}_\mu^* : \tilde{\mathbf{u}}_\mu(\boldsymbol{y}^+) = \tilde{\mathbf{u}}_\mu(\boldsymbol{y}^-) \; \forall \, \text{pairs } (\boldsymbol{y}^+, \boldsymbol{y}^-) \in \partial\Omega_\mu \right\} \tag{19}$$

  Again, only the zero body force field is orthogonal to the chosen space of fluctuations.

$$\mathbf{q}_\mu(\boldsymbol{y}^+) = -\mathbf{q}_\mu(\boldsymbol{y}^-) \quad \forall \text{ pairs } (\boldsymbol{y}^+, \boldsymbol{y}^-) \in \partial\Omega_\mu \tag{20}$$

- *Minimally constrained* or *Uniform RVE boundary traction model*. In this case, we chose

$$\mathcal{V}_\mu = \mathcal{V}_\mu^{\mathcal{U}} := \tilde{\mathcal{K}}_\mu^* \tag{21}$$

Again only the zero body force field is orthogonal to the chosen space. The boundary traction orthogonal to the space of fluctuations satisfies the *uniform boundary traction condition* (de Souza Neto and Feijóo, 2006):

$$\mathbf{q}_\mu(\boldsymbol{y}) = \mathbf{T}\mathbf{n}(\boldsymbol{y}) \quad \forall \boldsymbol{y} \in \partial\Omega_\mu \tag{22}$$

where $\mathbf{T}$ is the macro-scopic stress tensor defined in Equation 11.

2.2 The homogenized elasticity tensor

The assumed type of the material response in the micro-scale implies that the macro-scopic response is linear elastic. That is, there is a *homogenized elasticity tensor* $\mathbb{C}$ such that

$$\mathbf{T} = \mathbb{C}\,\mathbf{E} \tag{23}$$

A closed form for the homogenized constitutive tensor can be derived by the approach suggested by Michel et al. (1999) and relies on the representation of the RVE equilibrium problem (Equation 16) as a superposition of linear variational problems associated with the cartesian components of the macro-scopic strain tensor. The resulting expression for $\mathbb{C}$ reads

$$\mathbb{C} = \bar{\mathbb{C}} + \tilde{\mathbb{C}} \tag{24}$$

where $\bar{\mathbb{C}}$ is the volume average macro-scopic elasticity tensor

$$\bar{\mathbb{C}} = \frac{1}{V_\mu}\int_{\Omega_\mu} \mathbb{C}_\mu \tag{25}$$

and the contribution $\tilde{\mathbb{C}}$ (generally dependent upon the choice of space $\mathcal{V}_\mu$) is defined as

$$\tilde{\mathbb{C}} := \left[\frac{1}{V_\mu}\int_{\Omega_\mu} (\tilde{\mathbf{T}}_{\mu_{kl}})_{ij}\right](\mathbf{e}_i \otimes \mathbf{e}_j \otimes \mathbf{e}_k \otimes \mathbf{e}_l) \tag{26}$$

where $\tilde{\mathbf{T}}_{\mu_{ij}} = \mathbb{C}_\mu \nabla^s \tilde{\mathbf{u}}_{\mu_{ij}}$ is the fluctuation stress field associated with the fluctuation displacement field $\tilde{\mathbf{u}}_{\mu_{ij}} \in \mathcal{V}_\mu$ that solves the linear variational problem

$$\int_{\Omega_\mu} \mathbb{C}_\mu \nabla^s \tilde{\mathbf{u}}_{\mu_{ij}} \cdot \nabla^s \boldsymbol{\eta} = -\int_{\Omega_\mu} \mathbb{C}_\mu (\mathbf{e}_i \otimes \mathbf{e}_j) \cdot \nabla^s \boldsymbol{\eta} \quad \forall \boldsymbol{\eta} \in \mathcal{V}_\mu \tag{27}$$

for $i, j = 1, 2$ (in the two-dimensional case). In the above, $\{\mathbf{e}_i\}$ denotes an orthonormal basis for the two-dimensional Euclidean space.

For a more detailed description on the derivation of Expressions 24–27) we refer the reader to Michel et al. (1999); de Souza Neto and Feijóo (2006) and Giusti et al. (2009b).

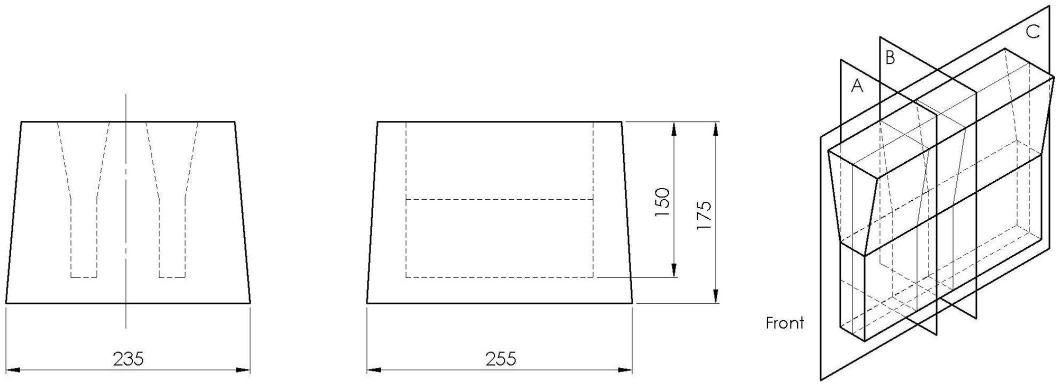

(a) Two views of double 1in. Y-block mold. (b) $3D$ view and cut's plane of 1in. Y-block.

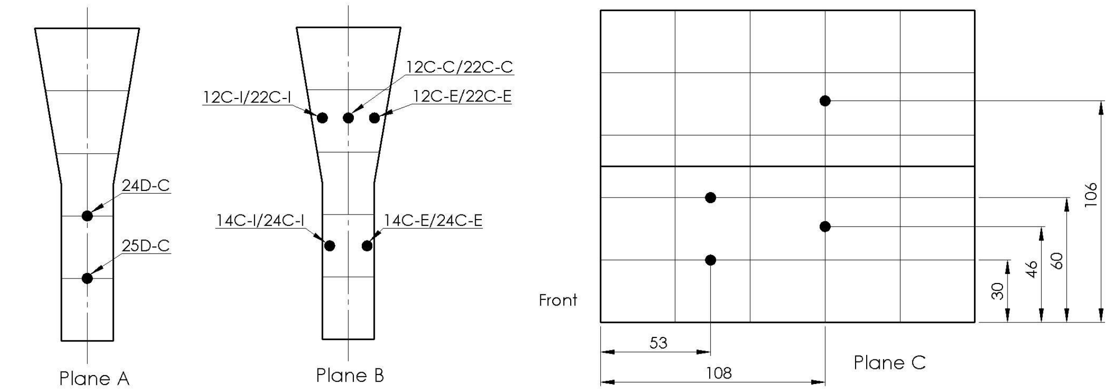

(c) Cut plane A. (d) Cut plane B. (e) Cut plane C.

Figure 4: Mold, 1in. Y-block and locations of the samples used for metallurgical study.

3 EXPERIMENTAL PROCEDURE

The micrographs used in the research were obtained from 1in Y-blocks (see Figure 4(a)) of slightly hypereutectic pearlite SGI. The alloy used in the experiments was melted in a high frequency induction furnace of 15 kN capacity. The load consisted of: 23.26% SAE 1010 steel scrap, 23.26% SGI scrap, 6.6% pig iron, 41.8% of the puddle. To adjust the carbon content was employed 1.6% carbon (90% performance), 2.0% of steel sheets and steel shavings, 0.15% of SiCa and to adjust the silicon content was added Fe75%Si. The base metal was overheated to 1650°C for a period of about 20 minutes. Inoculation and nodularization treatments were carried out following the Sandwich Method, in which the substances are placed in a ladle and are covered with steel sheets and steel shavings, and then the liquid metal is poured from the furnace (Elliot, 2005). The treatment of the liquid was carried out with the addition of 1.5% FeSiMgCe (nodulizant) and 0.7% Fe75%Si (post-inoculation treatment). The molten metal was subsequently poured into the ladle to fill the Y-blocks. Then, the blocks were divided into 25 parts as shown in Figure 4(e).

The main elements of the chemical composition of the cast alloy are listed in Table 2.

The location of the samples used in the analysis of the Y-blocks are shown in Figures 4(c), 4(d), and 4(e), and the points analyzed in each sample are indicated in Figure 4(c) and 4(d). The preparation of the samples consisted in the successive rough grinding using waterproof abrasive papers with grades ranging: 180, 240, 400, 600, 800 and 1000. Next, each sample was polished

Element	C	Si	Mn	P	S	Cr	Cu	Sn	Mg	CE
wt-%	3,55	2,78	0.49	0.012	0.010	0.023	0.89	0.010	0.054	4.52

Table 2: Average chemical composition (main elements) of samples, wt-%.

with diamond paste of granulometry of 6 μm. The samples were observed under an optical microscope Olympus PMG 3 equipped with a video camera connected to a computer.

The micrography were processed with a analyzer program of object. the result is three image (original than improved illumination, segmented and with contour of nodules detected, see Figures 6 to 9), more the necessaries information for construct the element finite mesh. For the implementation of hexagonal RVE, we cut the original micrography with a regular hexagon inscribed. The mesh was create with program called GMSH (Geuzaine and Remacle, 2009).

The metallurgical study consists in the determination of graphite and metal matrix volume fraction (the last is a mixture of ferrite and pearlite), and the graphite phase characterization which consists in the determination of size and roundness of each nodule and corresponding main and minor axis from the ellipse interpolated from each nodule. From the above measurements, the nodularity corresponding to each sample was calculated from SinterCast (1997):

$$Nodularity = \frac{\sum_{i=1}^{nodules} A_i + 0.5 \sum_{j=1}^{intermediates} A_j}{\sum_{k=1}^{nodules>10\mu m} A_k} 100 \tag{28}$$

where A_i, A_j and A_k are the surface areas of *nodules* whose roundness is greater than 0.625, *intermediates* nodules whose roundness is greater than 0.525 and less than 0.625 (see Figure 5), and all nodules of the sample with diameter which is greater than 10 μm, respectively. In our case, the major axis of all nodules are greater than 10 μm. Note that the above expression is able to obtain the nodularity of the SGI, for the case of compacted and flake graphite see SinterCast (1997).

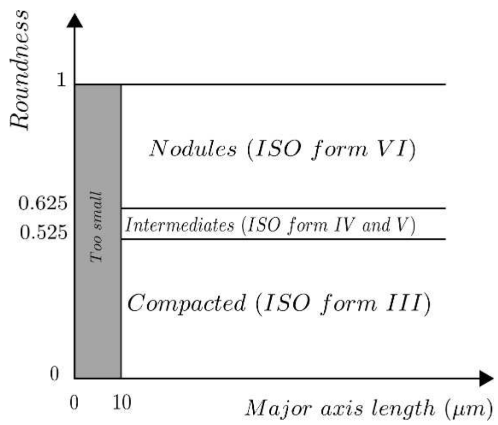

Figure 5: Classification of graphite nodules (SinterCast, 1997).

Figure 5 shows the classification of graphite nodules according to roundness, which is calculated as follows (Castro et al., 2003):

$$Roundness = \frac{4\pi S}{P} \tag{29}$$

where S and P are the surface and perimeter of nodules respectively.

For compacted graphite cast irons the nodularity is typically in the range of $0-10\%$, whereas that for SGI, the nodularity is approaching 100% and for flake graphite and according to SinterCast (1997) a nodularity of -5% describes a fully lamellar graphitic structure. The graphite Young's modulus varies as a function of nodularity according to (Sjogren, 2007)

$$E_i = 0.173Nodularity + 18.9 \tag{30}$$

Applying Equation 30 for the case of SGI with 100% nodularity, the graphite Young modulus is $36.2\ GPa$.

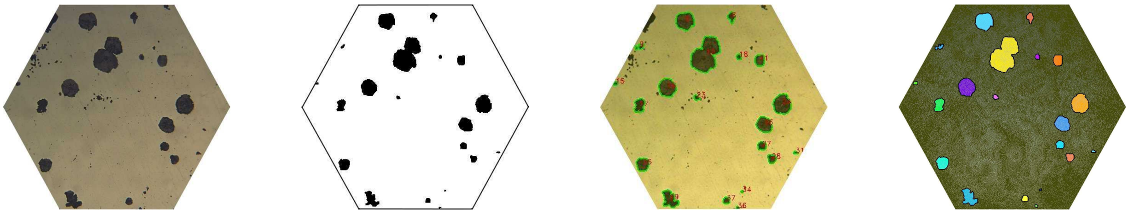

(a) Original. (b) Segmented. (c) Nodule contours. (d) FEM mesh.

Figure 6: Images corresponding to $14C \times 100\_E$ hexagonal sample (see Figure 4(d)).

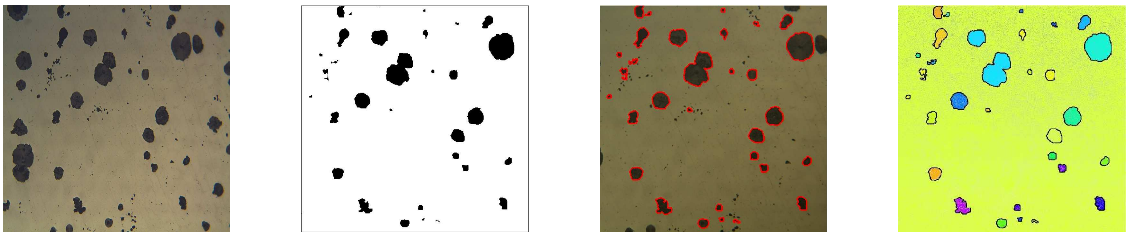

(a) Original. (b) Segmented. (c) Nodule contours. (d) FEM mesh.

Figure 7: Images corresponding to $14C \times 100\_E$ rectangular sample (see Figure 4(d)).

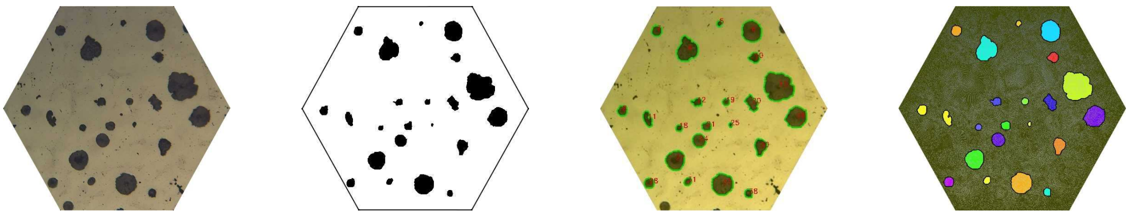

(a) Original. (b) Segmented. (c) Nodule contours. (d) FEM mesh.

Figure 8: Images corresponding to $14C \times 100\_I$ hexagonal sample (see Figure 4(d)).

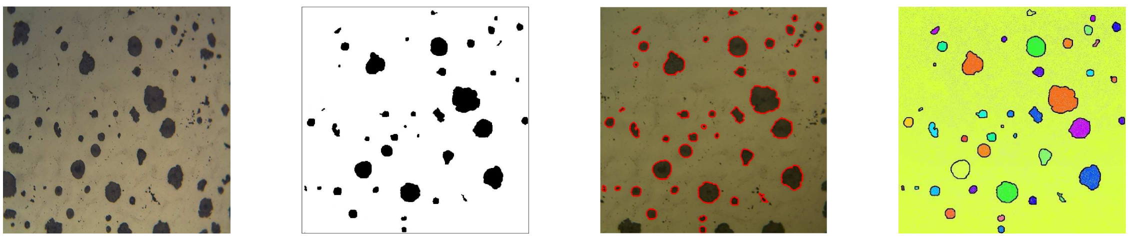

(a) Original. (b) Segmented. (c) Nodule contours. (d) FEM mesh.

Figure 9: Images corresponding to $14C \times 100\_I$ rectangular sample (see Figure 4(d)).

4 RESULTS AND DISCUSSION

The aim of this section is to present the obtained results from the multi-scale analysis using two diferents RVE (hexagonal and rectangular) and a comparison with the classical analytical expression of the Young's modulus for SGI as mentioned in the previous section. The analytical expression in which this work is based is given by

$$E_{eff} = E_m \left\{ 1 - \frac{\pi}{A} \left[1 - \frac{1}{9\left(1 + \frac{1.99}{B}\left\{\frac{E_m}{E_i} - 1\right\}\right)} - \frac{1}{3\left(1 + \frac{1.68}{B}\left\{\frac{E_m}{E_i} - 1\right\}\right)} - \frac{5}{9\left(1 + \frac{1.04}{B}\left\{\frac{E_m}{E_i} - 1\right\}\right)} \right] \right\}, \tag{31}$$

with

$$A = \frac{\left(\frac{4\pi}{3c_i}\right)^{2/3} ar^{-1/3}}{\sqrt{1 + (ar^{-2} - 1)\cos^2\alpha_i}} \quad \text{and} \quad B = \left(\frac{4\pi}{3c_i}\right)^{1/3} ar^{1/3}\sqrt{1 + (ar^{-2} - 1)\cos^2\alpha_i} \tag{32}$$

where E_{eff}, E_m, and E_i, are the Ypung's modules of the cast iron, the matrix and the inclusion of graphite, respectively; c_i is the volume fraction of the graphite, ar is the aspect ratio of the inclusions, and $\cos^2\alpha_i$ describe the orientation of the inclusions. For the special case of random statistical orientation $\cos^2\alpha_i = 0.33$. A detailed explanation of this expression is given by Boccaccini (1997).

In the resolution of the set of variational problems (Equation 27), for each multi-scale model described in Section 2.1, the numerical procedure described in Giusti et al. (2009a) was used. The finite element mesh used was build with triangular linear elements. The numbers of elements and nodes used in each FEM's mesh are shown in Table 3.

Sample	Rectangular RVE		Hexagonal RVE	
	Elements	Nodes	Elements	Nodes
12Cx100_C	406900	204477	250764	126130
12Cx100_E	421760	211907	250142	125287
12Cx100_I	406940	204497	255752	128624
14Cx100_E	431388	216721	257098	129297
14Cx100_I	424174	213114	260652	131047
22Cx100_C	409826	205940	255012	128254
22Cx100_E	411134	206594	250142	125819
22Cx100_I	415094	208574	258536	130016
24Cx100_E	426040	214047	263504	132500
24Cx100_I	428000	215027	255002	128249
24Dx100	409552	205803	266450	133973
25Dx100	410132	206093	248574	125035

Table 3: Elements and nodes for the meshes for rectangular and hexagonal RVE.

The values of the parameters corresponding to the metallic matrix and graphite nodules used for the rectangular RVE are listed in Table 4 (Carazo et al., 2011).

Sample	Graphite vol. frac. (c_i)	Aspect ratio (as)	Nodularity %	Young's Modulus (GPa)		Poisson ratio	
				E_m	E_i	Matrix	Graphite
12Cx100_C	9.904	0.827	94.529	206	35.254	0.290	0.2225
12Cx100_E	7.728	0.834	98.047	206	35.862	0.290	0.2225
12Cx100_I	7.653	0.862	99.018	206	36.030	0.290	0.2225
14Cx100_E	7.247	0.736	88.275	206	34.172	0.290	0.2225
14Cx100_I	8.252	0.799	94.114	206	35.182	0.290	0.2225
22Cx100_C	11.605	0.852	88.049	206	34.133	0.290	0.2225
22Cx100_E	9.183	0.835	97.359	206	35.743	0.290	0.2225
22Cx100_I	8.898	0.824	95.765	206	35.467	0.290	0.2225
24Cx100_E	8.043	0.776	92.581	206	34.916	0.290	0.2225
24Cx100_I	8.328	0.758	98.405	206	35.924	0.290	0.2225
24Dx100	7.703	0.797	97.223	206	35.721	0.290	0.2225
25Dx100	11.905	0.819	97.542	206	35.775	0.290	0.2225

Table 4: Constitutive properties of the metal matrix (ferrite plus pearlite) and graphite used in the simulations for rectangular RVE.

Sample	Graphite vol. frac. (c_i)	Nodularity %	Young's Modulus (GPa)				
			Taylor	Linear	Periodic	Uniform	Eq. 31
12Cx100_C	9.904	94.529	189.089	172.606	171.639	169.617	174.686
12Cx100_E	7.728	98.047	192.852	179.480	178.709	177.176	180.252
12Cx100_I	7.653	99.018	192.992	179.838	179.449	178.632	180.082
14Cx100_E	7.247	88.275	193.548	180.195	179.410	177.042	182.629
14Cx100_I	8.252	94.114	191.904	177.014	176.761	175.856	179.280
22Cx100_C	11.605	88.049	186.055	166.455	165.123	162.487	169.613
22Cx100_E	9.183	97.359	190.365	174.187	173.553	172.483	176.477
22Cx100_I	8.898	95.765	190.826	175.770	175.295	174.296	177.308
24Cx100_E	8.043	92.581	192.240	177.621	176.887	175.559	180.138
24Cx100_I	8.328	98.405	191.836	177.235	176.391	174.748	180.058
24Dx100	7.703	97.223	192.884	179.019	178.104	176.206	180.862
25Dx100	11.905	97.542	185.735	166.601	165.486	164.003	170.271

Table 5: Results corresponding to the differents models and Equation 31 for rectangular RVE.

The numerical results for rectangular RVE corresponding to the different classes of multi-scale constitutive models (Sub-section 2.1), and for Equation 31, are presented in Table 5 and ploted in Figures 10 and 11 (Carazo et al., 2011).

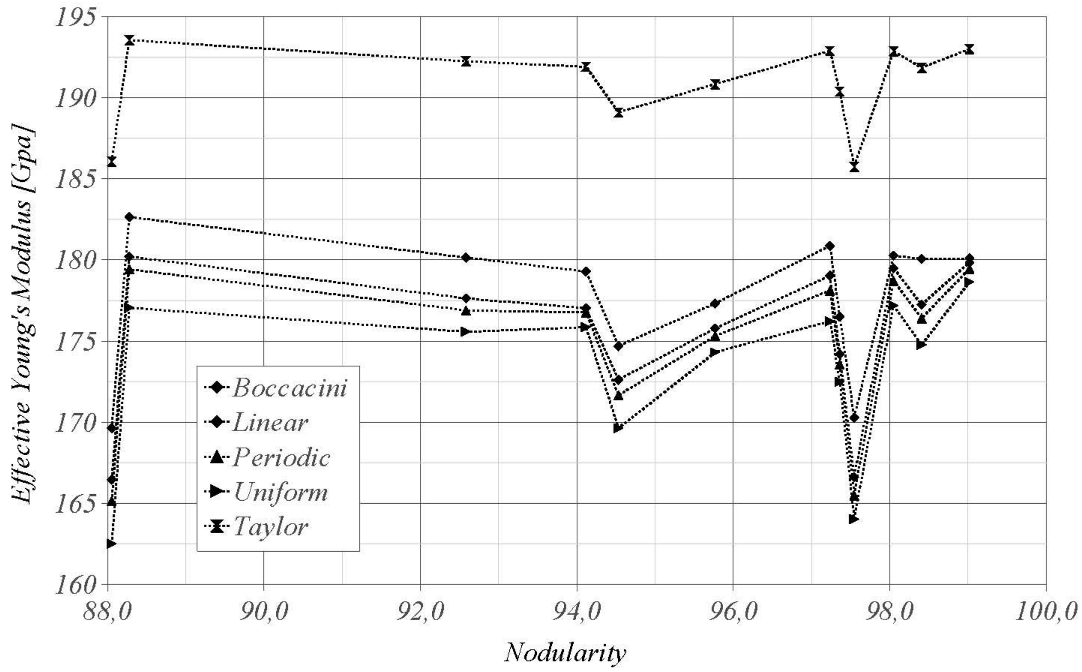

Figure 10: Comparison of the results of multi-scale simulation for rectangular RVE and Equation 31.

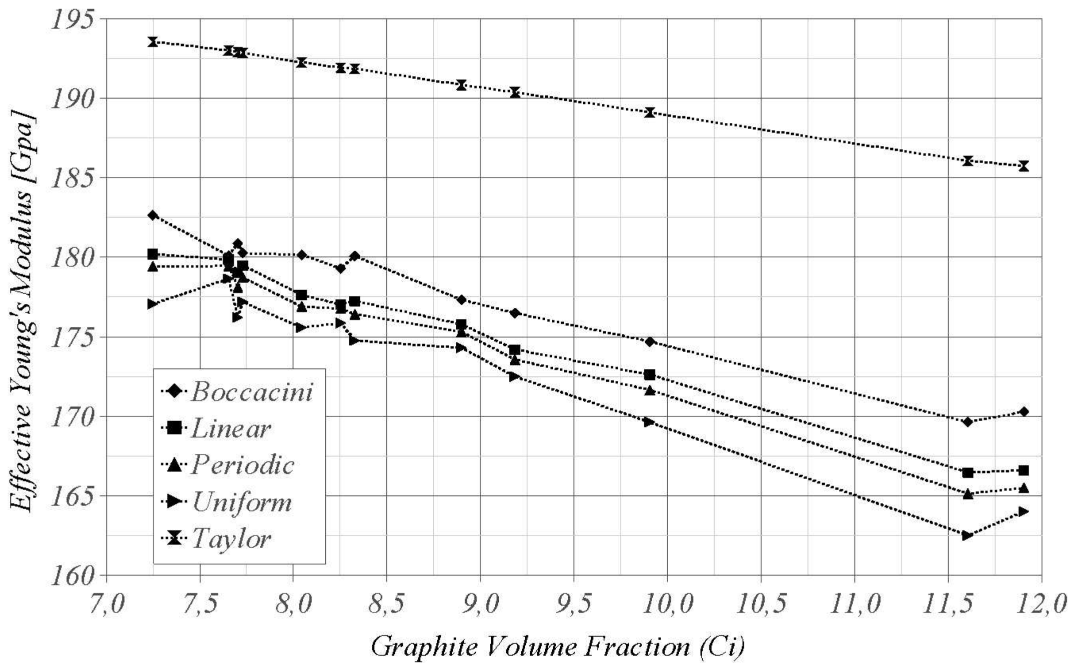

Figure 11: Comparison of the results of multi-scale simulation for rectangular RVE and Equation 31.

The values of the parameters corresponding to the metallic matrix and graphite nodules used for hexagonals RVEs are listed in Table 6.

Sample	Graphite vol. frac. (c_i)	Aspect ratio (as)	Nodularity %	Young's Modulus (GPa)		Poisson ratio	
				E_m	E_i	Matrix	Graphite
12Cx100_C	9.326	0.825	93.543	206	35.083	0.290	0.2225
12Cx100_E	7.983	0.846	99.823	206	36.169	0.290	0.2225
12Cx100_I	7.321	0.884	99.342	206	36.086	0.290	0.2225
14Cx100_E	6.890	0.794	98.481	206	35.937	0.290	0.2225
14Cx100_I	10.097	0.851	95.427	206	35.409	0.290	0.2225
22Cx100_C	12.990	0.815	77.176	206	32.251	0.290	0.2225
22Cx100_E	10.511	0.849	97.856	206	35.829	0.290	0.2225
22Cx100_I	10.059	0.837	97.319	206	35.736	0.290	0.2225
24Cx100_E	9.490	0.782	91.095	206	34.659	0.290	0.2225
24Cx100_I	9.742	0.785	99.180	206	36.058	0.290	0.2225
24Dx100	8.661	0.838	100.000	206	36.200	0.290	0.2225
25Dx100	14.119	0.815	96.484	206	35.592	0.290	0.2225

Table 6: Constitutive properties of the metal matrix (ferrite plus pearlite) and graphite used in the simulations for hexagonal RVE.

Sample	Graphite vol. frac. (c_i)	Nodularity %	Young's Modulus (GPa)				
			Taylor	Linear	Periodic	Uniform	eq.31
12Cx100_C	9.326	93.543	190.061	173.866	173.114	171.957	176.095
12Cx100_E	7.983	99.823	192.442	178.469	177.850	177.179	179.490
12Cx100_I	7.321	99.342	193.560	181.245	180.743	179.375	180.676
14Cx100_E	6.890	98.481	194.283	181.359	180.376	179.237	183.065
14Cx100_I	10.097	95.427	188.775	171.273	170.246	169.043	173.805
22Cx100_C	12.990	77.176	183.430	160.801	159.920	157.231	166.511
22Cx100_E	10.511	97.856	188.113	170.279	169.505	168.202	172.966
22Cx100_I	10.059	97.319	188.872	172.502	171.807	170.542	174.270
24Cx100_E	9.490	91.095	189.739	173.652	171.743	168.802	176.397
24Cx100_I	9.742	99.180	189.445	172.817	172.178	171.091	176.197
24Dx100	8.661	100.000	191.293	176.820	175.487	173.813	177.900
25Dx100	14.119	96.484	181.939	160.435	159.008	155.981	165.331

Table 7: Results corresponding to the differents models and Equation 31 for hexagonal RVE.

The numerical results for hexagonal RVE corresponding to the different classes of multi-scale constitutive models (Sub-section 2.1) and for Equation 31, are presented in Table 7 and ploted in Figures 12 and 13.

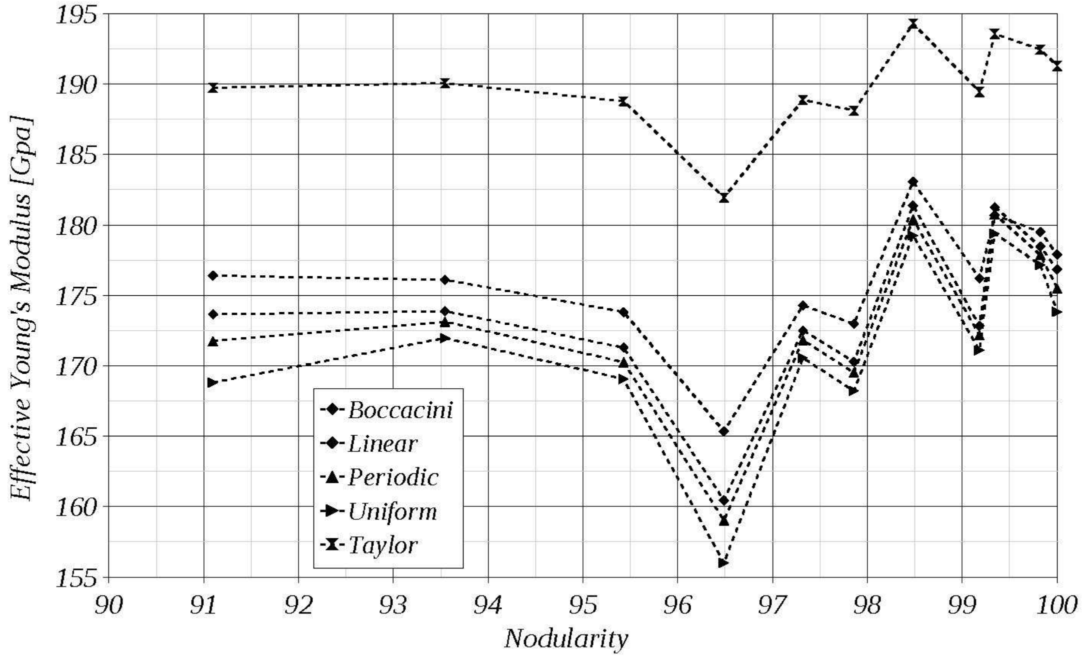

Figure 12: Comparison of the results of multi-scale simulation for hexagonal RVE and Equation 31.

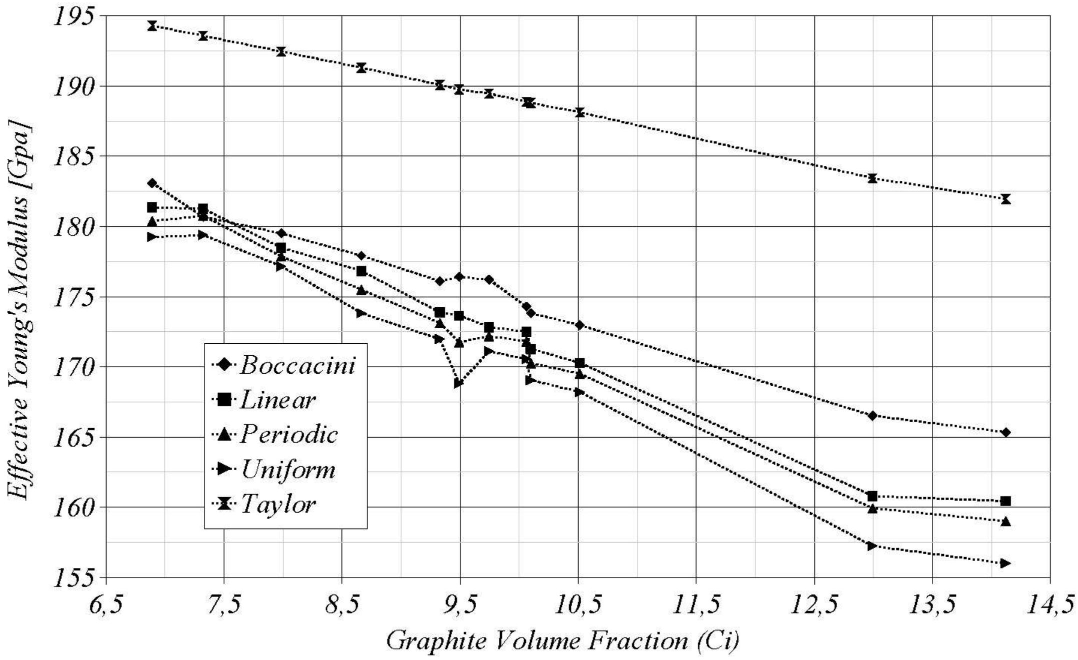

Figure 13: Comparison of the results of multi-scale simulation for hexagonal RVE and Equation 31.

As can see in Figures 10 to 13, the Boccaccini's model is most rigid for both kinds of RVEs used in the simulation with exception of Taylor's model.

On the other hand and as can see in the Figure 14 to 16; for linear, periodic and uniform models, the hexagonal RVE has Young's module slightly greater than rectangular RVE for volumetric graphite fraction equal to 11.5%. For volumetric graphite fraction greater than 11,5%, the behavior is reversed. Should be clarified, the volumetric graphite fraction is not very greater than 14% for the SGI.

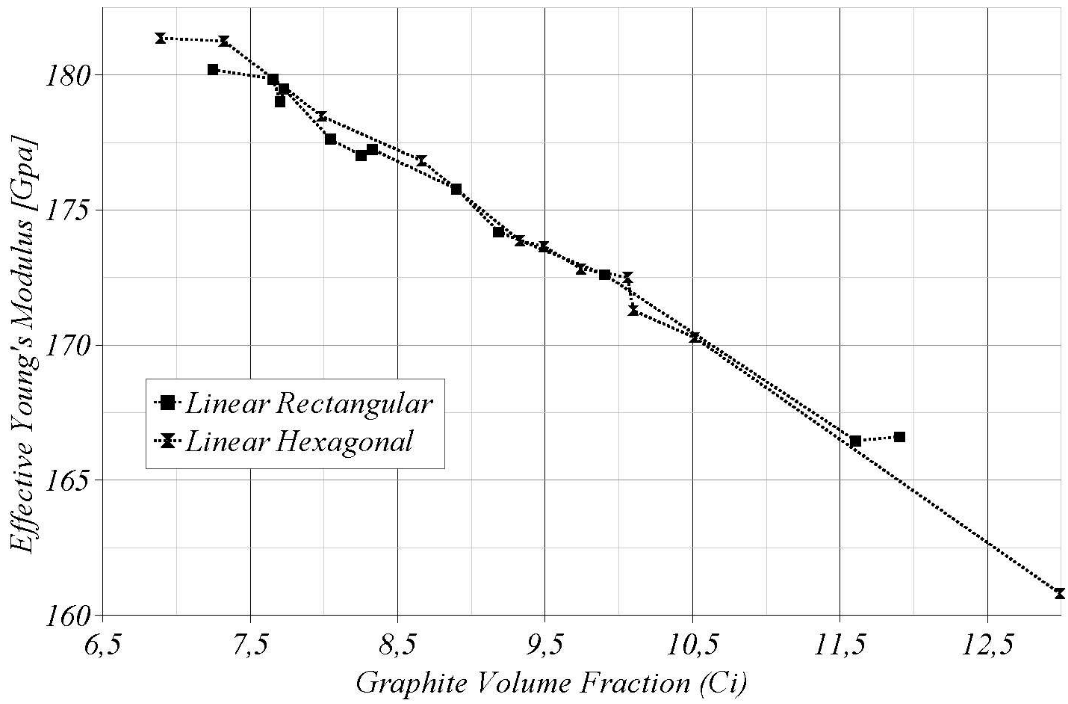

Figure 14: Comparison of the results of linear multi-scale simulation for rectangular and hexagonal RVE.

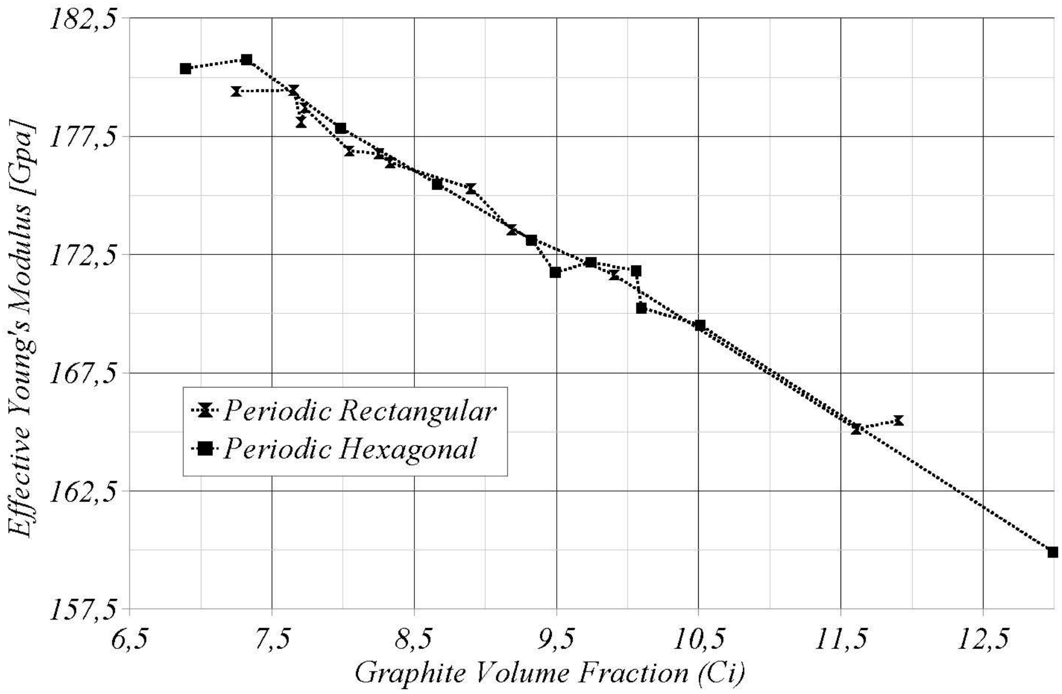

Figure 15: Comparison of the results of periodic multi-scale simulation for rectangular and hexagonal RVE.

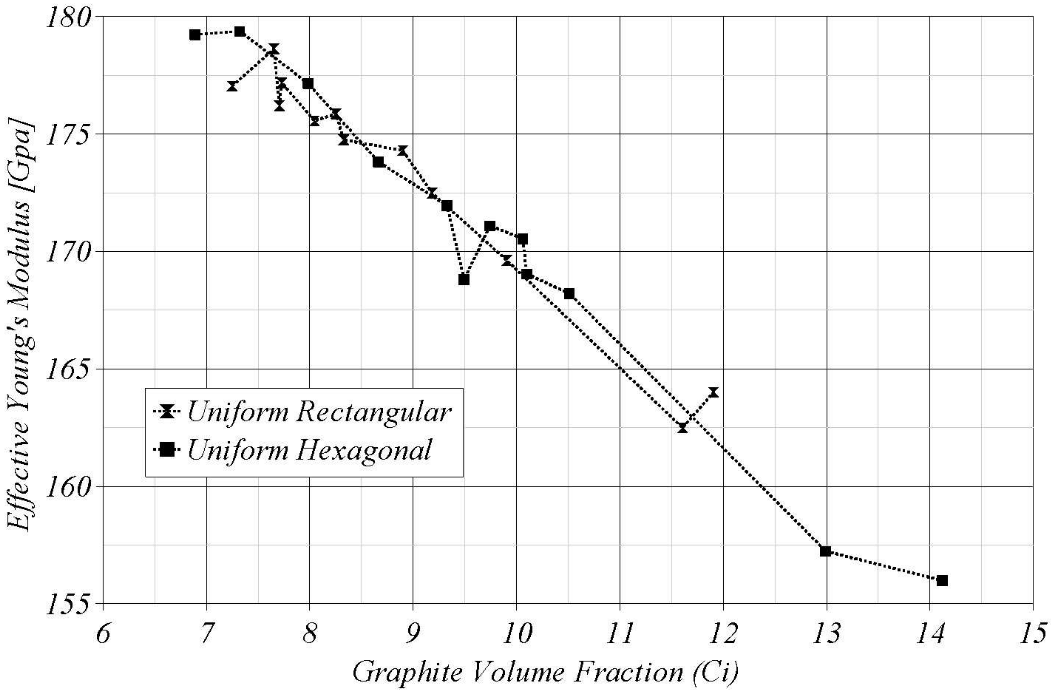

Figure 16: Comparison of the results of uniform multi-scale simulation for rectangular and hexagonal RVE.

5 CONCLUSIONS

A comparison between a classical analytical expression for the effective Young's modulus and the results of a computationally-based multi-scale analysis has been presented in this paper by using two shapes for the RVE (rectangular and hexagonal). A set of the micrograph was enhanced and segmented to obtain the volume fraction of metallic matrix and graphite phase and the boundary of each object. With this information, a finite element mesh was constructed, for each image. The multi-scale model is based in a classical homogenization procedure over a variational framework. For this work, only the linear elasticity model was used in the derivation of the macro-scopic Young's modulus.

For the analyzed RVEs, the constitutive response of the hexagonal RVE is most rigid than the rectangular RVE for a volumetric graphite fraction less than 11.5%, for a greater fraction the behavior is reversed. This conclusion holds for all the multi-scale models.

The results obtained indicate a good match of the analytical expression with the classical linear boundary displacement multi-scale model. For the other models investigated, the difference never exceeded the 5%. This difference indicates that the analytical expression given by Equation 31 could be used in an engineering application for prediction of the effective elastic parameter. However, for an accurate estimate of the macro-scopic Young's modulus, a more detailed multi-scale study is needed. In particular, it is necessary take into account, among others, the shape and size of the RVE. These aspects are currently under investigation.

ACKNOWLEDGEMENTS

This research was partly supported by Ministry of Science, Technology and Productive Innovation of Argentina, National Technological University - Regional Faculty of Cordoba (UTN-FRC) and the National Council of Scientific and Technical Research (CONICET). A.D. Boccardo has been partly supported by CONICET doctoral program. We would like to thank Jorge

Sánchez from CIEM-CONICET, for many helpful discussions and support in the image software develop. The melt used in this research were made at the company that produces gray and nodular cast iron, Sánchez - Piccioni, located in the city of Alma Fuerte, Province of Córdoba, Argentina. This support is gratefully acknowledged.

REFERENCES

ASTM A536. Standard specification for ductile iron castings. 2009.

Bensoussan A., Lions J., and Papanicolau G. *Asymptotic analysis for periodic microstructures*. North Holland, Amsterdam, 1978.

Berryman J.G. and Blair S.C. Kozeny-carman relations and image processing methods for estimating darcy's constant. *Journal of Applied Physics*, 62:2221–2228, 1987.

Boccaccini A.R. Effect of graphite inclusions on the young's modulus of cast iron. *Zeitschrift für METALLKUNDE*, 88(1):23–26, 1997.

Bochenek B. and Pyrz R. Reconstruction methodology for planar and spatial random microstructures. In R. Pyrz, S. Schjodt-Thomsen, J.C. Rauhe, T. Thomsen, and L.R. Jensen, editors, *International conference on new challenges in mesomechanics*, pages 565–572. Danish technical research council, Aalborg, Denmark, 2002.

Bohm H.J., Rammerstorfer F., Fischer F., and Siegmund T. Microscale arrangement effects on the thermomechanical behavior of advanced two-phase composites. *Journal of Engineering Materials and Technology*, 116:268–273, 1994.

Carazo F., Giusti S., Boccardo A., Dardati P., and Godoy L. Characterization of nodular cast-iron using multi-scale constitutive modeling. *Mecánica Computacional*, xxx(8):611–629, 2011.

Castro M., Herrera-Trejo M., Alvarado-Reyna J.L., Martínez-Tello C.L., and Méndez-Nonell M. Characterization of graphite form in nodular graphite cast iron. *International Journal of Cast Metals Research*, 16(1-3):83–86, 2003.

de Souza Neto E. and Feijóo R. Variational foundations of multi-scale constitutive models of solid: small and large strain kinematical formulation. Technical Report No 16/2006, Laboratório Nacional de Computação Científica LNCC/MCT, Petrópolis, Brasil, 2006.

Deve H.E. Effect of fiber spatial arrangement on the transverse strength of titanium matrix composites. *Metallurgical Transactions A*, 30:2513–2522, 1999.

Drugan W. and Willis J. A micromechanics-based nonlocal constitutive equation and estimates of representative volume element size for elastic composites. *Journal of the Mechanics and Physics of Solids*, 44:497–524, 1996.

Elliot R. *Cast Iron Technology*. Jaico Publishing House, 2005.

Evesque P. Fluctuations, correlations and representative elementary volume (rev) in granular materials. *Poudres Grains*, 11:6–17, 2000.

Fischmeister H.F. and Karlsson B. PlastizitÂÍtseigenschaften grob-zweiphasiger werkstoffe. *Metallurgical Transactions A*, 68:311–327, 1977.

Germain P., Nguyen Q., and Suquet P. Continuum thermodynamics. *Journal of Applied Mechanics, Transactions of the ASME*, 50(4):1010–1020, 1983.

Geuzaine C. and Remacle J.F. Gmsh: a three-dimensional finite element mesh generator with built-in pre- and post-processing facilities. *International Journal for Numerical Methods in Engineering*, 79(11):1309–1331, 2009.

Ghosh S. and Moorthy S. Elastic-plastic analysis of arbitrary heterogeneous materials with the voronoi cell finite element method. *Computational Methods in Applied Mechanics Engineering*, 121(1-4):373–409, 1995.

Gitman I.M., Askes H., and Sluys L. Representative volumen: Existence and size determination. *Engineering Fracture Mechanics*, 74(16):2518–2534, 2007.

Giusti S., Blanco P., de Souza Neto E., and Feijóo R. An assessment of the Gurson yield criterion by a computational multi-scale approach. *Engineering Computations*, 26(3):281–301, 2009a.

Giusti S., Novotny A., de Souza Neto E., and Feijóo R. Sensitivity of the macroscopic elasticity tensor to topological microstructural changes. *Journal of the Mechanics and Physics of Solids*, 57(3):555–570, 2009b.

Hashin Z. Analysis of composite materials a survey. *Journal of Applied Mechanics*, 50:481–505, 1983.

Hill R. Elastic properties of reinforced solids: some theoretical principles. *Journal of the Mechanics and Physics of Solids*, 11:357–372, 1963.

Hill R. A self-consistent mechanics of composite materials. *Journal of the Mechanics and Physics of Solids*, 13(4):213–222, 1965.

Hollister S.J. and Kikuchi N. Homogenization theory and digital imaging: a basis for studying the mechanics and design principles of bone tissue. *Biotechnology and Bioengineering*, 43(7):586–596, 1994.

Li M., Ghosh S., Richmond O., Weiland H., and Rouns T.N. Three dimensional characterization and modeling of particle reinforced metal matrix composites, part i: Quantitative description of microstructural morphology. *Materials Science and Engineering A*, 265:153–173, 1999.

Mandel J. *Plasticité classique et viscoplasticité*. CISM Lecture Notes. Springer-Verlag, Udine, 1971.

Mazilu P. and Ondracek G. On the effective young's modulus of elasticity for porous materials. part i: The general model equation. In K. Herrmann and Z. Olesiak, editors, *Thermal effects in fracture of multiphase materials. Proceedings of Euromechanic 255 Colloquium*, pages 214–255. Springer-Verlag, Paderborn, FRG, 1990.

Michel J., Moulinec H., and Suquet P. Effective properties of composite materials with periodic microstructure: a computational approach. *Computer Methods in Applied Mechanics and Engineering*, 172(1-4):109–143, 1999.

Miehe C., Schotte J., and Schröder J. Computational micro-macro transitions and overall moduli in the analysis of polycrystals at large strains. *Computational Materials Science*, 16(1-4):372–382, 1999.

Ostoja-Starzewski M. Material spatial randomness: From statistical to representative volume element. *Probabilistic Engineering Mechanics*, 21:112–132, 2006.

Panchal S. Indian foundry industry. 2010.

Rintoul M. and Torquato S. Reconstruction of the structure of dispersions. *Journal of Colloid and Interface Science*, 186:467–476, 1997.

Roberts A.P. and Garboczi E.J. Elastic properties of a tungstens-silver composite by reconstruction and computation. *Journal of the Mechanics and Physics of Solids*, 47:2029–2055, 1999.

Sanchez-Palencia E. *Non-homogeneous media and vibration theory*, volume 127 of *Lecture Notes in Physics 127*. Springer-Verlag, Berlin, 1980.

SinterCast. *SinterCast Nodularity Rating Chart*. SinterCast, 1997.

Sjogren T. *Influences of the graphite phase on elastic and plastic deformation behaviour of cast irons*. Ph.D. thesis, INSTITUTE OF TECHNOLOGY, Department of Management and Engineering, Division of Engineering Materials, Linköping University, Jönköping, Sweden, 2007.

Terada K. and Kikuchi N. Microstructural design of composites using the homogenization method and digital images. *Materials Science Research International*, 2:65–72, 1996.

Torquato S. Morphology and effective properties of disordered heterogeneous media. *International Journal of Solids and Structures*, 35:2385–2406, 1998.

Trusov P.V. and Keller I. The theory of constitutive relations. part i. *Perm: Perm State Technical University*, 1997.

van Mier J. *Fracture processes of concrete*. CRC Press, Inc., 1997.

Zeman J. and Sejnoha M. Numerical evaluation of effective elastic properties of graphite fiber tow impregnated by polymer matrix. *Journal of the Mechanics and Physics of Solids*, 49:69–90, 2001.